OPTOELECTRONICS AND ADVANCED MATERIALS – RAPID COMMUNICATIONS Vol. 5, No. 12, December 2011, p. 1272 - 1276

SiO_2 passivation layer fabricated by inline oxidation for silicon solar cells

SONG ZHANG[a], ZHENJIAO WANG[c], XI XI[b], JINGJIA JI[c,d], GUOHUA LI[a,d,*]
[a]*School of Science, Jiangnan University, Wuxi 214122, China*
[b]*School of Internet of Things Engineering, Jiangnan University, Wuxi 214122, China*
[c]*Suntech Power Co. Ltd., Wuxi 214028, China*
[d]*Jiangsu (Suntech) Institute for Photovoltaic Technology, Wuxi 214028, China*

In this paper, it is demonstrated that the inline oxidation utilizing inline diffusion equipment is an extremely promising alternative to the application of classical quartz tube furnace for thin SiO_2 film growth. The results reveal that the thin SiO_2 passivation layer fabricated by inline oxidation has a suitable thickness (~10 nm) and provides sufficient passivation, which has a very high thermal stability, and little interference with the antireflection system. Both inline oxidation and tube oxidation show similar results in minority carrier lifetime with and without SiN_x layer. Utilizing the inline oxidation process, solar cells with thin SiO_2/SiN_x stack passivation layer front side and all Al-BSF rear side, obtained an efficiency of 18.3%, while the efficiency was only 17.59% of the cells with single SiN_x layer.

(Received November 10, 2011; accepted November 23, 2011)

Keywords: Silicon solar cells, Inline oxidation, Thin SiO_2 film, Passivation

1. Introduction

Currently, fabricating high efficiency and low-cost silicon solar cells is one of main issues in the photovolatic field. Surface passivation is a crucial factor in crystalline silicon solar cells since it significantly contributes to the efficiency of cells [1, 2]. High temperature (900 -1100) thermal silicon dioxide (SiO_2) has been used in solar cell process for many years, especially in high-efficiency solar cells, such as PERL (Passivated Emitter, Rear Locally diffused), PERT (Passivated Emitter, Rear Totally diffused), and PLUTO [3-5]. SiO_2 film is usually formed by classical furnace oxidation (CFO) or rapid thermal oxidation (RTO). CFO is generally used for laboratory high-efficiency solar cells for passivation [6, 7]. RTO process is very fast (<5 min) and an efficiency of 18.6% can be reached with 12 nm SiO_2 film [8]. But the growth of passivation layer mentioned above is normally produced in a quartz tube furnace, manual loading system. This method results in a higher breakage and cost. So the inline oxidation process is a very promising alternative to conventional quartz tube furnaces for the passivation of industrial phosphorus-diffused emitters. Currently, the inline technologies are mainly used on the diffusion [9-11] or PECVD (Plasma-enhanced Chemical Vapour Deposition) [12-14]. There are few relevant reports on the inline oxidation, especially using existing inline diffusion equipments [10].

The aim of the work is to comprehensively study the thermal growth of SiO_2 film by the in-line diffusion equipment and the application of thin thermal oxide film in solar cells based on inline oxidation. Furthermore, the passivation properties of the inline oxide/silicon nitride stack layer are investigated. Finally, the chosen optimal passivation layers are applied to fabricate solar cells.

2. Experiments

In this work 1-3Ω•cm p-type <100> 125mm×125mm Cz (Czochralski) mono-Si wafers of 200±10 μm thickness were used. The silicon wafers were cleaned following the RCA (Radio Corporation of American) standard clean procedure [7] before inline-oxidation process. All the mono-Si samples were texturized in alkaline solution. The emitter with sheet resistance 53Ω/□ was formed at 865 for 25 min in a diffusion furnace. After diffusion the phosphorus silicate glass (PSG) and parasitic junction were removed by wet chemical etching. Then the samples were divided into several groups and different thermal oxidation processes were applied. For the inline-oxidation, the SiO_2 film was achieved by the in-line diffusion equipment using the optimal oxidation process. The same oxidation atmospheres of dry oxygen were applied for the CFO and inline oxidation processes. The oxidation temperature and time were adapted to different oxidation type, but did not surpass 900 . The targeted oxide layer thickness was 10~15 nm. The SiN_x layers were deposited by a parallel plate plasma-enhanced chemical vapor deposition system made by Roth & Rau.

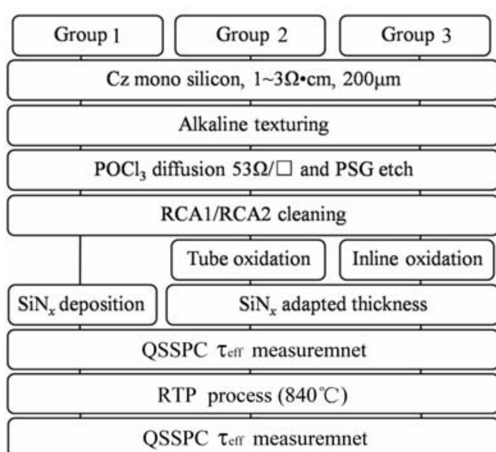

Fig. 1(a). Process sequence for the preparation of test structures.

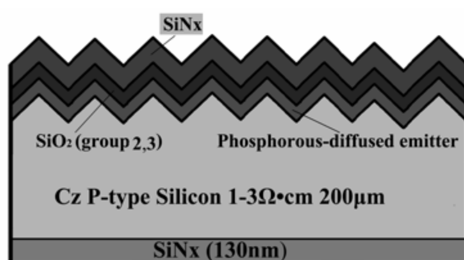

Fig. 1(b). Schematic sketch of the test structure.

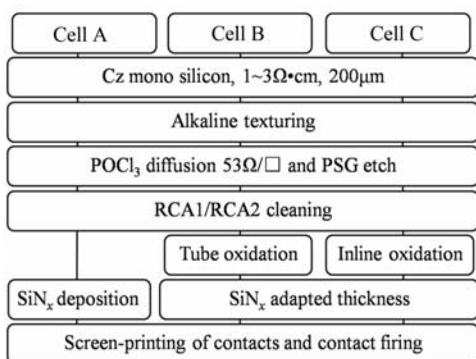

Fig. 2 (a). Process sequence for the preparation of Al-BSF solar cells.

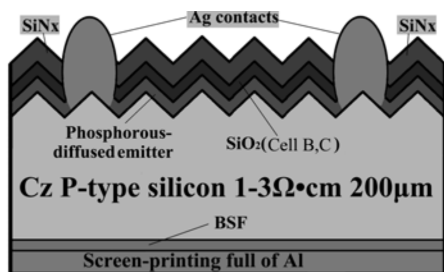

Fig. 2 (b). Sketch cross section of the solar cell structure.

The process flow for the preparation of lifetime samples and the sketch of fabricated samples for different pasivation layers are illustrated in Fig. 1. To evaluate the inline oxidation on solar cell level, the fabrication of solar cell process flow and the sketch of solar cells are showed in Fig. 2. Before SiN_x deposition, the sheet resistance of all samples is about 83 Ω/☐, eliminating the difference in phosphorous diffusion profile.

The reflectivity (R) and quantum efficiency (QE) measurement were carried out by spectral response measurement system (produced by PV Measurements Inc.). The thicknesses of the SiO_2 film and SiN_x film were measured by an ellipsometer (produced by Gaertner Scientific Corporation). The minority carrier lifetime has been obtainde by a Quasi-Steady-State Photoconductance (QSSPC) lifetime measurement system (model WCT-120 from Sinton Instrument). After printing the front and backside metallization, the samples were sintered in a belt furnace. The solar cells I-V characteristics were measured by IV tester system (produced by IVT Solar Pte Ltd.) under standard conditions of AM1.5G at cell temperature of 25 .

3. Results and discussion

3.1 Minority carrier lifetime

The minority carrier lifetime was measured immediately after inline oxidation process. Fig. 3 shows variations in τ_{eff} with an increase in minority carrier lifetime before and after oxidation, and after forming gas annealing (FGA). It is obvious that after inline oxidation the sample has a τ_{eff} of 31 μs while before oxidation it is only 12 μs. After annealing in forming gas at 400 for 25min, the lifetime reaches 40 μs. For the tube oxidation, the τ_{eff} are 33.91 μs and 43 μs respectively after oxidation and FGA process. Remarkably, the inline oxidation process yields similar minority carrier lifetime to the tube oxidation process, after oxidation and FGA process, from Fig. 3. The limited difference of minority carrier lifetime between tube oxidation and inline oxidation seems to be related to the phosphorus-doped profile, which will have a little effect on the passivation of emitter.

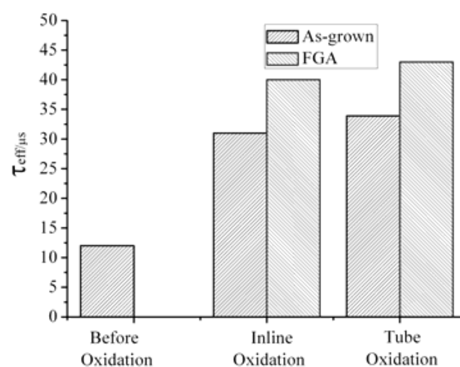

Fig. 3. The effective carrier lifetime with thermal SiO_2 film.

This significant improvement of lifetime before and after oxidation can be ascribed the reducing of the surface states density, via SiO_2 passivation. As a result of the SRH (Shockley-Read-Hall) theory [15], the τ_{eff} largely depends on the surface states (defects and dangling bonds). With the thermal grown silicon oxide on the wafer surface, the dangling bonds on the surface drop rapidly, so the effective minority carrier lifetime has an increase of 9 µs and 9.09 µs respectively.

Compared to the thermal-grown state, the interface state density can be drastically reduced by annealing in forming gas at 400 [16]. At the interface of Si/SiO_2 there exists a very thin (<2 nm) interfacial region with nonstoichiometric suboxides. This region is considered to be the site of defects causing interface states, namely, surface recombination centers [7]. The hydrogen atoms in forming gas infiltrate into the Si/SiO_2 interface through the SiO_2 film to saturate the dangling silicon bonds, and provide good hydrogen passivation effect [17, 18]. Additionally, the field effect passivation mechanism is another reason for the increasing of minority carrier lifetime. But in this work, the SiO_2 film is very thin (10~15nm), and SiO_2 layer contains a quite low fixed charge density Q_f which resulting in no or only a weak inversion layer [19]. So the τ_{eff} increase is more effectively reached for thermal grown SiO_2 layer, and it appears to be the key factor in passivation.

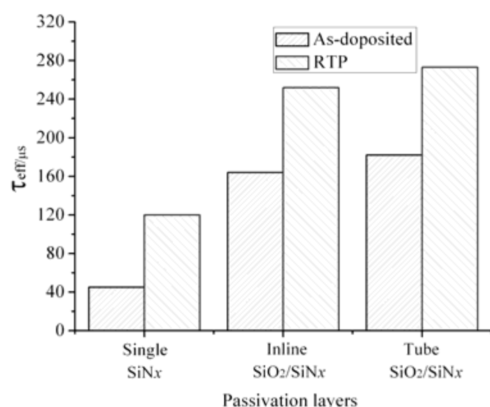

Fig. 4. Compared of effective carrier lifetime achieved with different passivation layers.

The surface passivation by inline thermal SiO_2/SiN_x stack layer and single SiN_x layer were also investigated with the tube thermal SiO_2/SiN_x layer as a reference sample. As shown in Fig. 4, with single SiN_x layer, the τ_{eff} is only 45 µs. After rapid thermal process (RTP), the τ_{eff} increases to 120 µs. For the inline thermal SiO_2/SiN_x stack layer, the τ_{eff} is 164µs, and after RTP process, the sample exhibits a high τ_{eff} up to 252 µs. For the tube thermal SiO_2/SiN_x reference sample, the τ_{eff} is similar with the inline thermal SiO_2/SiN_x stack layer, 182 µs and 273 µs respectively before and after RTP process.

The effective lifetime of the samples employing inline thermal and tube thermal thin SiO_2/SiN_x stack layer is substantially higher than that of samples with a single SiN_x layer, as shown in Fig. 4. It is obvious that the structure of the double layers is different from the single SiN_x layer. This leads to different passivation mechanisms, and therefore difference in saturation of interface dangling bonds. This can be explained by the high quality of the Si/SiO_2 interface, which is grown on the silicon crystal surface at high temperature, and the subsequent effective hydrogenation of interface states during the SiN_x deposition [20]. For the single SiN_x layer, the deposition of such layer induces passivation of silicon dangling bonds at the surface. On the other hand, a high positive fixed charge density Q_f is present in the SiN_x layer, which allows reducing the minority carrier concentration at the Si/SiN_x interface by means of field-effect passivation [21]. So, the improvement of τ_{eff} for SiO_2/SiN_x stack layer can be attributed to a combined effect of advantage of both thin thermal oxide and nitride layers, the low D_{it} at the Si/SiO_2 and the high Q_f, which act as field-effect passivation and a source of hydrogen for dangling bonds passivation [22].

Additionally, after the RTP process (temperature: 840 , time: 20s), the τ_{eff} has an increase about 167%, 54% and 50% for single SiN_x layer, inline thermal SiO_2/SiN_x stack layer and tube thermal SiO_2/SiN_x stack layer respectively. This phenomenon can be ascribed to hydrogenation in the nitride layer. Annealing at temperature above the deposition temperature, the Si-H bonds and N-H bonds are broken. The release of hydrogen in its atomic form consequently leads to an efficient passivation of silicon dangling bonds at the interface and the bulk defects of Si substrate [21].

3.2 Application to solar cells

Fig. 5 shows the reflectance, external quantum efficiency (EQE) and internal quantum efficiency (IQE) of solar cells fabricated with single SiN_x layer and SiO_2/SiN_x stack layer (between Cell A, Cell B and Cell C) in the wavelength range 350-1100 nm.

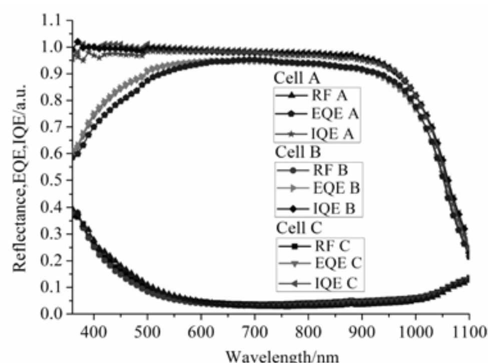

Fig. 5. Quantum efficiency (EQE) and reflectance of the solar cells (A: single SiN_x layer, B: tube SiO_2/SiN_x stack layer, C: inline thermal SiO_2/SiN_x stack layer).

The reflectance curves of the different coating layers are similar over the large range of wavelength. The QE curves from Fig. 5 show that cells with stack layer have higher QE in the 350-600 nm wavelength range than that with single SiN_x coating, especially the EQE. And the Cells (Cell B and Cell C) with SiO_2/SiN_x stack layer have similar QE in the wavelength range 350-1100 nm. Although the single SiN_x layer has a good optical property, the surface state density D_{it} at Si/SiN_x interfaces is much larger than in the case of thermally grown Si/SiO_2 interfaces [23]. With the thin SiO_2 interlayer, the SiO_2/SiN_x stack layer shows a smaller interface defect density (D_{it}) than that in Si/SiN_x interface [24], which results in a better blue response. Besides of this, in the co-firing of solar cells in the belt furnace during fabrication process, hydrogen can be released from SiN_x film and some of them penetrate into the silicon bulk and Si/SiO_2 interface, which provides hydrogen passivation of the defects [25].

Table 1. Comparison of solar cell parameters fabricated using single SiN_x layer and SiO_2/SiN_x stack layer.

No.	V_{oc} (mV)	J_{sc} (mA/cm^2)	FF (%)	η (%)
Cell A	616.8	36.24	78.7	17.59
Cell B	634	37.36	77.9	18.47
Cell C	628.9	37.12	78.38	18.3

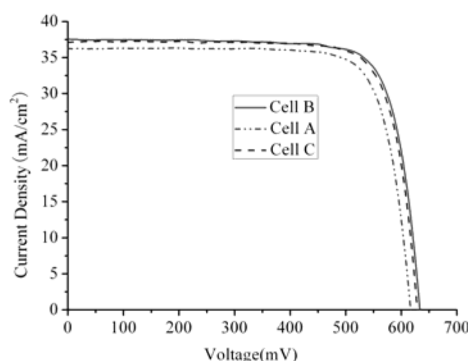

Fig. 6. J-V curves of solar cells with different passivation layers (A: single SiN_x layer, B: tube SiO_2/SiN_x stack layer, C: inline thermal SiO_2/SiN_x stack layer).

Table 1 illustrates a comparison of the cell parameters fabricated with single SiN_x layer and SiO_2/SiN_x stack layer. Corresponding J-V curves are showed in Fig 6. Table 1 shows that the cell fabricated with inline thin SiO_2/SiN_x stack layer have a superior conversion efficiency of 18.3% (Cell C) while the sample with a single SiN_x layer shows only the efficiency of 17.59% (Cell A). Furthermore, the cell with inline thermal thin SiO_2/SiN_x stack layer has a high short circuit current density (J_{sc}) of 37.12 mA/cm^2, which is 0.88 mA/cm^2 higher than that of the cell with a single SiN_x layer. The high J_{sc} value is primarily contributed to good passivation of the stack layer, because the reflectance curves of the different coating layers are quite similar over a large range of wavelengths (showed in Fig. 5). As a buffer layer between Si and SiN_x film, the thin SiO_2 film will reduce the stress of Si/SiN_x interface. Moreover, the Si/SiO_2 interface has lower interface states density than that of the Si/SiN_x interface, and the application of thin SiO_2 film enhances the adhesion of stack system on silicon [7]. So, the thin SiO_2 film provides sufficient passivation effect and dose not interfere with the optical system of antireflection.

In addition, the open circuit voltage (V_{oc}) of cells with inline thermal thin SiO_2/SiN_x stack layer shows an increase by 12.1 mV (absolute value) compared to that of the cell with single-layer coating due to a better emitter passivation [26]. For the little FF difference between Cell B and C seems to be related to the slight change of the phosphorous diffusion profile during oxidation.

Compared with CFO process, the solar cell (Cell B) by simple inline oxidation process presents a similar result, as shown in Fig. 6. Although there exists a little difference in J-V parameters, it is estimated that the wafers are contaminated from metal mesh belt, which is made of nichrome alloy, and the risk of metal contamination is high [10]. Nevertheless, the performances of cells with inline thermal SiO_2 film and CFO SiO_2 film are similar, and better than that with single SiN_x layer coating.

4. Conclusions

In this work, the growth of thin SiO_2 film produced by inline oxidation and its application in solar cells were investigated. The samples passivated with inline thermal thin SiO_2 film and SiO_2/SiN_x stack layer yield similar minority carrier lifetime compared with the CFO process. For the application in solar cells, both of the inline oxidation process and CFO process illustrate similar in RF and QE, but there is a little difference in J-V parameters. It is estimated that the primary reason is the metal contamination due to metal mesh belt being made from nichrome alloy, so the advanced transport mechanism that does not cause wafer contamination and inefficient energy consumption is necessary. Overall, the inline oxidation process is a promising alternative to the CFO process for solar cell manufacturing.

Acknowledgment

The authors acknowledge the equipment support of research and development department, suntech power corporation, Ltd.

Reference

[1] G. Claudia, K. Bass, K. Heasman, A. Cole, S. Roberts, S. Watson, M. Boreland, Superlattices and Microstructures **45**, 234 (2009).
[2] C. Boehme, G. Lucovsky, Journal of Non-Crystalline Solids **299-302**, 1157 (2002).
[3] Z. Jianhua, W. Aihua, M. A. Green, Solar Energy Materials & Solar Cells **65**, 429 (2001).
[4] S. Narayanan, S. R. Wenham, M. A. Green, IEEE Transactions on Electron Devices **37**(2), 382 (1990).
[5] S. Zhengrong, S. R. Wenham, J, Jingjia, 34th IEEE Photovoltaic Specialists Conference, Philadelphia, USA, 1922-1926 (2009).
[6] J. Knobloch, S. W. Glunz, D. Biro, W. Warta, E. Schăffer, W. Wettling, Conference Record of the 25th IEEE Photovoltaic Specialists Conference **4**, 405-408 (1996).
[7] G. A. Aberle, Crystalline Silicon solar cells: Advanced Surface Passivation and Analysis, Centre for Photovoltaic Engineering, University of New South Wales, Sydney (2004).
[8] P. Doshia, A. Rohatgia, M. Roppa, Z. Chena, D. Rubyb, D. L. Meier, Solar Energy Materials & Solar Cells **41-42**, 31 (1996).
[9] D. Biro, R. Preu, G. Willeke, D. Untiedt, G. Wander, J. Gentischer, 19th European Photovoltaic Solar Energy Conference, Paris, France, June, 7-11 (2004).
[10] P. J. Richter, F. J. Bottari, D. C. Wong, 35th IEEE PVSC, Honolulu, Hi, USA, June, 3593-3596 (2010).
[11] J. Hoornstra, W. V. Strien, M. Lamers, 22nd European Photovoltaic Solar Energy Conference and Exhibition, September, Milan, Italy, 3-7 (2007).
[12] H. P. Sperlich, D. Decker, P. Saint-Cast, E. Erben, L. Peters, 25th European Photovoltaic Solar Cell Energy Conference and Exhibition/5th World Conference on Photovoltaic Energy Conversion, Valencia, Spain, September, 6-10 (2010).
[13] M. C. Wei, S. J. Chang, C. Y. Tsia, C. H. Liu, S. C. Chen, Solar Energy **80**, 215 (2006).
[14] J. Bultman, J. Hoornstra, Y. J. Komatsu, I. Romijn, A. Stassen, K. Tool, Photovoltaics International 5th edition, September, **2**(3), 77 (2009).
[15] J. Y. Lee, Rapid Thermal Processing of silicon solar cells - Passivation and Diffusion. PhD Thesis, University of Freiburg (2003).
[16] H. Jin, K. J. Weber, P. J. Smith, Journal of the Electrochemical Society **154**(6), H417 (2007).
[17] I. Babak, L. L. Fee, G. P. Harold, J. M. Anthony, IEEE Transctions on Electron Devices, **57**(4), 877 (2010).
[18] I. M. Obaidat, N. Qamhieh, J. Optoelectron. Adv. Mater. **9**(10), 3268 (2007).
[19] J. Y. Lee, S. W. Glunz, Solar Energy Material & Solar Cells **90**, 82 (2006).
[20] Y. Larionova, V. Mertens, N. P. Harder, R. Brendel, Applied Physics Letters **96**, 032105 (2010).
[21] J. –F. Lelièvre, E. Fourmond, A. Kaminski, O. Palais, D. Ballutaud, M. Lemiti, Solar Energy Material & Solar Cells **93**, 1281 (2009).
[22] E. Simoen, C. Gong, N. E. Posthuma, E. V. Kerschaver, J. Poortmans, R. Mertens, Journal of the Electrochemical Society **158**(6), H612 (2011).
[23] G. A. Aberle, Progress in Photovoltaics Research and Applications, **8**, 473 (2000).
[24] K. C. Sinje, B. Nadine, S. Christian, S. Andreas, S. Dominik, S. Petra, M. Stefan, B. Dietmar, 26th European PV Solar Energy Conference and Exhibition, Hamburg, Germany, September, 5-9 (2011).
[25] S. Gatz, T. Dullweber, V. Mertens, F. Mertens, F. Einsele, R. Brendel, Solar Energy Materials and Solar Cells, In Press (2011).
[26] S. W. Glunz. Advances in OptoElectronics, 2007, 1 (2007).

*Corresponding author: guohua_li55@yahoo.com